Eur. Phys. J. D **41**, 641–654 (2007)
DOI: 10.1140/epjd/e2006-00262-4

THE EUROPEAN PHYSICAL JOURNAL D

Test ion acceleration in a dynamic planar electron sheath

M.M. Basko[a]

Institute for Theoretical and Experimental Physics, B. Cheremushkinskaya 25, 117218 Moscow, Russian Federation

Received 21 August 2006 / Received in final form 13 October 2006
Published online 8 December 2006 –

Abstract. New exact results are obtained for relativistic acceleration of test positive ions in the laminar zone of a planar electron sheath evolving from an initially mono-energetic electron distribution. The electron dynamics is calculated against the background of motionless foil ions. The limiting gamma-factor $\gamma_{p\infty}$ of accelerated ions is shown to be determined primarily by the values of the ion-electron charge-over-mass ratio $\mu = m_e Z_p/m_p$ and the initial gamma-factor γ_0 of the accelerated electrons. For $\mu > 1/8$ a test ion always overtakes the electron front and attains $\gamma_{p\infty} > \gamma_0$. For $\mu < 1/8$ a test ion can catch up with the electron front only when γ_0 is above a certain critical value γ_{cr}, which for $\mu \ll 1$ can most often be evaluated as $\gamma_{cr} = (1/4)\mu \exp\left(\mu^{-1} - 1\right)$. In this model the protons and heavier test ions, for which $\gamma_{cr} > 10^{398}$ is enormous, always lag behind the front edge of the electron sheath and have $\gamma_{p\infty} < \gamma_0$; for their maximum energy an appropriate intermediate asymptotic formula is derived. The domain of applicability of the laminar-zone results is analyzed in detail.

PACS. 52.38.Kd Laser-plasma acceleration of electrons and ions – 52.40.Kh Plasma sheaths

1 Introduction

One of the most impressive latest achievements in the laser plasma physics has been the observation of well-collimated high-energy proton and ion beams produced from thin metallic foils irradiated by ultra-intense sub-picosecond laser pulses [1–4]. An exceptional quality, demonstrated recently for thus produced proton beams [5], makes them very promising for many potential applications [6].

In its gross features, the mechanism of ion acceleration in the cited and other similar experiments is believed to be reasonably well understood, and has been nicknamed TNSA (target normal sheath acceleration) [7,8]. High directionality and low phase volume of generated protons [5] indicate that they are accelerated in a highly ordered electric field normal to the virtually unperturbed planar rear surface of a laser-irradiated foil. The electric field is caused by charge separation in the sheath layer that is formed by energetic electrons generated by absorption of the laser pulse.

However, an attempt to provide a more detailed and comprehensive theoretical description leads to a very complex system of plasma dynamics equations that can hardly be ever solved rigorously. To establish practically useful dependences and relations, one has to introduce additional simplifications. As is typical in many areas of physics, of particular value for gaining a deeper understanding of the process of ion acceleration prove to be certain particular idealized but exactly solvable problems. Salient and well known examples are (i) a self-similar evolution of the ion distribution function by quasi-neutral plasma expansion into vacuum [9], and (ii) an exact two-fluid solution of the isothermal plasma expansion with a full account of charge separation effects [10]. Recently, solutions have also been published [11–13] which describe expansion of finite plasmas into vacuum. In this paper we present a rigorous solution and full parametric analysis of another such idealized problem, namely, the problem of test ion acceleration in a dynamic electron sheath with the delta-function initial velocity distribution.

Typically, fast protons in laser irradiated metallic foils originate from a thin (few nanometers) contaminant layer of water and hydrocarbons at the foil surface [3,4,14]. Then, a natural simplification would be to assume that the heavy bulk ions (like Au for example) of a metallic foil are infinitely heavy and stay at rest, while the accelerated protons are treated as test positive charges initially located at the foil surface. Our present solution is essentially based on this assumption.

Next, one has to choose how to treat the electrons. A widely used assumption is that the electrons instantaneously relax to the equilibrium Boltzmann distribution in the time-dependent electrostatic potential of the expanding plasma: it was employed in all the solutions [9–13] cited above. With immobile ions, such an assumption allows straightforward calculation of the electrostatic sheath potential $\phi(x)$ either in the one-temperature [15] or multi-temperature [16] cases. An obvious problem with this approximation is that it leads to a diverging result for the

[a] e-mail: basko@itep.ru

maximum energy of accelerated test ions because the corresponding potential $\phi(x) = -(2T/e)\ln\left[1 + x/(\sqrt{2}\lambda_D)\right]$ [15] logarithmically diverges at $x \to +\infty$ in the planar geometry; here λ_D is the Debye length at the base of the electron sheath with temperature T, $+e$ is the elementary charge. However, as was pointed out by Gurevich et al. [9], this divergence is not physical because even if one assumes that the hot electrons have a perfect Maxwellian distribution initially, at $t = 0$, it still takes an increasingly long time $\Delta t \simeq t_{eq}(x) \propto x$ for the Boltzmann relation $n_e \propto \exp(e\phi/T)$ to establish at an increasingly large distance x from the initial plasma surface (for more details see Sect. 3.2.2 below). As possible remedies, attempts have been made to use ad hoc quasi-equilibrium electron distributions truncated either at high velocities [17,18] or at large distances [19]. Evidently, neither of these two approaches is fully self-consistent.

Without the Boltzmann relation, a self-consistent treatment requires that one starts with a given initial electron distribution function at $t = 0$, and then calculates its evolution for $t > 0$. For high-energy (multi-MeV) electrons this can be done in the collisionless approximation. In this work we solve this problem in the simplest case of initially monoenergetic electrons, i.e. when at $t = 0$ all the free electrons of a uniform planar foil acquire one and the same initial velocity v_0 perpendicular to the foil. Rigorous results are obtained for the one-dimensional test ion acceleration in the outer laminar zone (defined in Sect. 3.1 below) of the dynamically evolving planar electron sheath. Particular attention is paid to the limiting energy of accelerated ions at $t \to \infty$, which is always finite within the adopted model.

This paper is not the first publication addressing thus formulated problem: to a significant extent, it builds upon earlier work by Bulanov et al. [20]. The new progress made here includes the following key issues. Temporal behavior of the boundary between the outer laminar and the inner relaxation zones of the dynamically evolving electron sheath is studied in detail. Consequently, the domain of applicability of the laminar-zone results for test ions is clearly identified in the full parameter space of the problem. In contrast to reference [20], the electric field in the laminar zone is calculated exactly, and not to the accuracy of the linear in x term. It is proven that the answer to the intriguing question of whether a test ion can overtake the electron front (and, consequently, surpass the initial electron velocity v_0) is determined by a critical relationship between the initial gamma-factor γ_0 of the accelerated electrons and the ion-electron charge-over-mass ratio μ [defined in Eq. (1) below]. A fully relativistic intermediate asymptotic formula (58) is derived which may be used in realistic situations to evaluate the maximum energy of accelerated protons and heavier ions.

2 Formulation of the problem

Consider a uniform planar and electrically neutral plasma layer (a metallic foil) of thickness l_0 with an initial density of free electrons n_0. At time $t = 0$ all the free electrons are set in motion with the same initial velocity v_0 perpendicular to the foil (see Fig. 1); v_0 can be arbitrarily close to the speed of light c. At later times $t > 0$ the motion of electrons, treated as a collisionless charged fluid, is governed by the electric field $E(t, x)$, which arises due to charge separation in the evolving plasma cloud. The origin of the x-axis, directed along the initial electron velocity $\boldsymbol{v}_0$, is chosen at the forward foil surface, so that initially the foil occupies the region $-l_0 \le x \le 0$. The bulk foil ions are assumed to be infinitely heavy and staying at rest. Our goal is to calculate the motion of a test ion of charge $+eZ_p$ and mass m_p placed initially at the foil surface $x = 0$, which is accelerated by the electric field $E(t, x)$ in the positive direction of the x axis. Note that here and below m_p is not necessarily the proton mass.

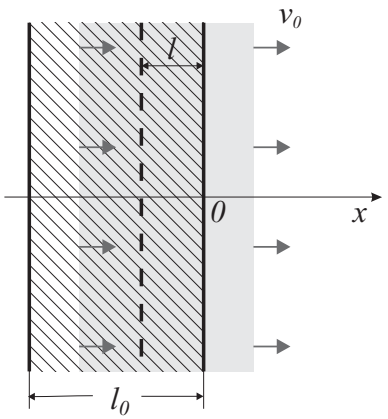

Fig. 1. Schematic view of a plasma foil with motionless bulk ions (hatched area) and electrons (grey area) boosted to a velocity v_0. Dashed vertical line marks the initial position of electrons with the Lagrangian coordinate l.

It is easy to understand that this problem is governed by only three independent dimensionless parameters, which we choose to be

$$\mu = \frac{m_e Z_p}{m_p}, \quad \Lambda = \frac{l_0\omega_0}{v_0\sqrt{\gamma_0}}, \quad \gamma_0 = (1-\beta_0^2)^{-1/2}; \qquad (1)$$

here m_e is the electron mass,

$$\omega_0 = \left(\frac{4\pi e^2 n_0}{m_e}\right)^{1/2} \qquad (2)$$

is the plasma frequency in the initial configuration, e is the positive elementary charge, and $\beta_0 = v_0/c$. If a proton (or some other light ion) is chosen as a test particle, the charge-over-mass ratio μ is small, $\mu \le 1/1836 \ll 1$. We will, however, explore the entire possible range of $0 < \mu < \infty$, firstly, for the sake of completeness of the analysis, and secondly, keeping in mind that light positive particles — like positrons, π^+ or μ^+ mesons — may in principle be created and accelerated under an intense laser irradiation.

For a non-thermal electron cloud considered here the quantity $v_0\sqrt{\gamma_0}/\omega_0$ plays a role of the Debye length. Then, the parameter Λ is the initial foil thickness in units of the Debye length. Of particular interest is the limit $\Lambda = 0$ of

a geometrically infinitely thin foil which, however, has a finite number

$$\Sigma = n_0 l_0 \tag{3}$$

of electrons per unit surface area. On the one hand, the effects of charge separation are the strongest in this limit for a given value of v_0. On the other hand, it is in this limit that most of the exact results can be established analytically; many of them are then straightforwardly extended to a more general case of $\Lambda \gtrsim 1$.

Parameter γ_0 is the relativistic gamma-factor of the accelerated electrons. In the non-relativistic limit of $\beta_0 \ll 1$, when $\gamma_0 \approx 1 + \beta_0^2/2$, this parameter becomes irrelevant, and we are left with only two principal parameters μ and Λ. On a par with β_0 and γ_0, the dimensionless momentum $\Pi_0 = \beta_0\gamma_0$ is used below as the principal kinematic characteristic of the accelerated electrons.

3 Motion of electrons

3.1 General notation and relationships

Motion of electrons is described by a function $x_e(t, l)$ [or by a function $x_e(t, \xi)$], where l (or ξ) is a Lagrangian coordinate in the electron fluid: $x_e(t, l)$ is the position at time t of an electron whose original position at $t = 0$ was $x_e(0, l) = -l$ (the dashed line in Fig. 1). The dimensionless Lagrangian coordinate $0 \le \xi \le 1$ is defined as

$$\xi = \frac{l}{l_0}. \tag{4}$$

Then, the front edge of the electron cloud is at $\xi = 0$, its rear edge is at $\xi = 1$.

At any fixed time t one can invert $x_e(t, \xi)$ with respect to ξ to obtain the inverse function $\xi = \xi(t, x)$ defined inside the expanding electron cloud. Without electron-electron collisions the function $\xi(t, x)$ ceases to be single-valued with respect to x after some time — even if it were so initially. In this paper we use the term "laminar zone" for that region of the electron cloud where $\xi(t, x)$ is single-valued (see Figs. 2 and 3 below). In the remaining "relaxation zone", where $\xi(t, x)$ is multi-valued, electrons gradually relax to the equilibrium Boltzmann distribution.

The function $x_e(t, \xi)$ is found by solving the following equations of electron motion

$$\frac{1}{c}\frac{dx_e}{dt} = \frac{\Pi_e}{\sqrt{1 + \Pi_e^2}} \equiv \beta_e, \tag{5a}$$

$$\frac{d\Pi_e}{dt} = -\frac{e}{m_e c}\, E(t, x_e), \tag{5b}$$

where $\beta_e = v_e/c$, and $\Pi_e = \beta_e\gamma_e = \beta_e(1 - \beta_e^2)^{-1/2}$; the Lagrangian time derivative d/dt is calculated at a fixed ξ. As is well-known, equations (5) admit an energy integral

$$m_e c^2 \Sigma \int_0^1 \gamma_e(t, \xi)\, d\xi + \frac{1}{8\pi}\int_{-\infty}^{+\infty} E^2\, dx = m_e c^2 \Sigma\, \gamma_0. \tag{6}$$

The electric field $E(t, x)$ is obtained by solving the Poisson equation, which in the planar geometry of our problem yields

$$E(t, x) = 4\pi e \Sigma\, [\sigma_e(t, x) - \sigma_i(x)]\,; \tag{7}$$

here $0 \le \sigma_e(t, x) \le 1$ [$0 \le \sigma_i(x) \le 1$] is the fraction of the total number of electrons (ions) above x at time t, i.e.

$$\sigma_e(t, x) = \frac{1}{\Sigma}\int_x^\infty n_e(t, x')\, dx'. \tag{8}$$

For motionless ions one obviously has

$$\sigma_i(x) = \begin{cases} 1, & x < -l_0, \\ -x/l_0, & -l_0 \le x \le 0, \\ 0, & x > 0. \end{cases} \tag{9}$$

Calculation of $\sigma_e(t, x)$ depends on whether x happens to be in the laminar or relaxation zone of the electron cloud. In the laminar zone one simply has $\sigma_e(t, x) = \xi(t, x)$, and the equations of motion (5) can be solved analytically.

In the relaxation zone, where the function $\xi(t, x)$ becomes multi-valued with respect to x, one has to use a more general expression

$$\sigma_e(t, x) = \sum_{x_e(t,\xi) > x} \Delta\xi, \tag{10}$$

where summation is done over all the segments $\Delta\xi$ which at time t are located inside the interval $(x, +\infty)$. Clearly, if equations (5) are to be solved with a full account of the relaxation zone, it can only be done numerically. To this end, a numerical code TIAC (test ion acceleration) has been written. This code is based on a routine explicit (with an appropriate time-step control) second-order discretization of equations (5), (7), (9), (10) combined with equations (38) for the ion motion. Such discretization poses no special difficulty since no partial derivatives with respect to ξ are involved. Interpenetration of different elements of the electron fluid is described straightforwardly by following the trajectories of a large number (typically a few thousand) of discrete points ξ_j along the Lagrangian variable ξ. Because of rapid randomization (for details see Sect. 3.2.2) of the electron motion at the core of the relaxation zone, such straightforward calculations can only be done within a limited time span of the order of 100 periods of electron oscillations near the foil surface.

3.2 Solution for $\Lambda = 0$

Here we consider the limit $l_0 \to 0$ of a geometrically very thin foil with a finite number of electrons per unit area $\Sigma = n_0 l_0$, where both the initial electron density n_0 and the plasma frequency ω_0 become formally infinite. In this case it is convenient to introduce the following units of time and length

$$[t] = t_\Sigma \equiv \frac{m_e v_0}{4\pi e^2 \Sigma}\,\gamma_0, \quad [x] = l_\Sigma \equiv v_0 t_\Sigma, \tag{11}$$

which replace the usual time and length scales $\sqrt{\gamma_0}/\omega_0$, $v_0\sqrt{\gamma_0}/\omega_0$ in a finite-density plasma. Evidently, the length unit l_Σ plays a role of the Debye length in our dynamic electron sheath. Below, the quantities measured in units (11) are marked with a bar. The electron trajectories are represented by a two-parameter family of curves $\bar{x}_e(\bar{t}, \xi, \beta_0)$.

3.2.1 Electron trajectories

In the laminar zone, where $\sigma_e = \xi$, equations (5) are solved analytically. The two relevant branches of this solution, obtained with the initial conditions $\bar{x}_e(0, \xi, \beta_0) = 0$, $\Pi_e(0, \xi, \beta_0) = \Pi_0 \equiv \beta_0\gamma_0$, are

$$\Pi_e = \Pi_0(1 - \xi\bar{t}), \tag{12a}$$

$$\bar{x}_e = \frac{\bar{t}(2 - \xi\bar{t})}{1 + \sqrt{1 - \beta_0^2\xi\bar{t}(2 - \xi\bar{t})}}, \tag{12b}$$

for $0 < \bar{t} < 2/\xi$, and

$$\Pi_e = \Pi_0\left[(1 - \xi)\bar{t} + 1 - 2/\xi\right], \tag{13a}$$

$$\bar{x}_e = \frac{\bar{t}^2(1 - \xi) + 2\bar{t}(1 - 2/\xi) + 4/\xi^2}{1 + \sqrt{1 - \beta_0^2\xi\bar{t}(2 - \xi\bar{t})}}, \tag{13b}$$

for $2/\xi < \bar{t} < 2/\left[\xi(1 - \xi)\right]$. In the upper half-space $\bar{x}_e > 0$ equation (12b) is easily inverted with respect to ξ, which leads us to the following expression for the electric field

$$E(\bar{t}, \bar{x}) = 4\pi e\Sigma\,\xi(\bar{t}, \bar{x}) = 8\pi e\Sigma\,\frac{\bar{t} - \bar{x}}{\bar{t}^2 - \beta_0^2\bar{x}^2}. \tag{14}$$

Inside the relaxation zone, where the electron trajectories intersect with one another, one has to abandon equations (12)–(14) and solve equations (5) numerically to calculate $\bar{x}_e(\bar{t}, \xi, \beta_0)$ and $E(\bar{t}, \bar{x})$.

For non-relativistic electrons $\bar{x}_e(\bar{t}, \xi) = \bar{x}_e(\bar{t}, \xi, 0)$ is a universal function of two variables $\bar{t}$ and ξ. It is plotted in Figure 2 for a selection of ξ values as calculated with the TIAC code. In Figure 3 the non-relativistic function $\bar{x}_e(\bar{t}, \xi)$ is plotted versus ξ for $\bar{t} = 20$. Qualitatively, the relativistic trajectories $\bar{x}_e(\bar{t}, \xi, \beta_0)$ look similar to $\bar{x}_e(\bar{t}, \xi, 0)$. In particular, for any $0 < \beta_0 < 1$ the rear edge of the electron cloud $\xi = 1$ turns around (i.e. has $\Pi_e = 0$) at $\bar{t} = 1$, and later crosses the foil at $\bar{t} = 2$ with $\Pi_e = -1$. For the period $0 < \bar{t} < 2$ there exists a vacuum gap between the foil ions and the ejected electrons. After its closure, the front and the rear edges of the electron cloud propagate freely in opposite directions with constant velocities $\pm v_0$.

Numerical solution of equations (5) enables one to trace the onset and subsequent expansion of the relaxation zone, shown in Figures 2 and 3 as shaded areas. In this zone oscillations of electrons around the positively charged foil, occurring on a time scale t_Σ, rapidly become stochastic and ultimately lead to establishment of the Maxwell-Boltzmann distribution with a certain temperature that can be found from the energy integral (6). The starting point of the relaxation zone can be calculated analytically

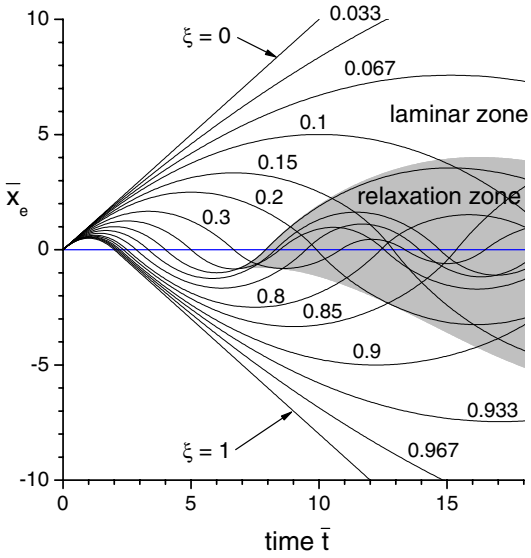

Fig. 2. Electron trajectories for $\Lambda = 0$ in the non-relativistic limit of $\beta_0 \ll 1$. Each curve is marked by the corresponding ξ value. The relaxation zone is shown as a grey shaded area.

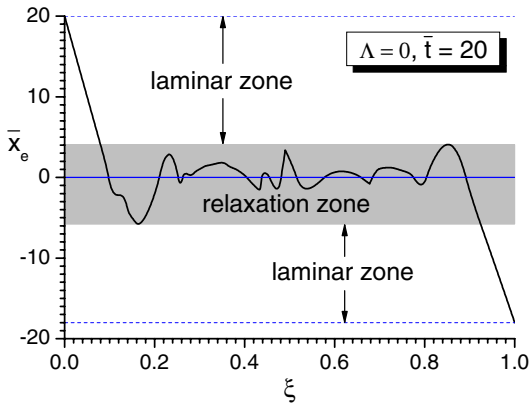

Fig. 3. Position of individual electrons $\bar{x}_e(\bar{t}, \xi)$ in the non-relativistic case at time $\bar{t} = 20$. Without electron-electron collisions, $\bar{x}_e(\bar{t}, \xi)$ is non-monotonic with respect to the Lagrangian coordinate ξ in the relaxation zone (shaded area). The number of local minima and maxima along ξ rapidly (exponentially) increases with time.

by applying the conditions $\partial\bar{x}_e/\partial\xi = 0$, $\partial^2\bar{x}_e/\partial\xi^2 = 0$ to equation (13b); in the non-relativistic limit it has the coordinates

$$\bar{t}_{r0} = \frac{27}{4}, \quad \xi_{r0} = \frac{4}{9}, \quad \bar{x}_{r0} = -\frac{27}{32}, \tag{15}$$

which become

$$\bar{t}_{r0} = 6, \quad \xi_{r0} = \frac{1}{2}, \quad \bar{x}_{r0} = -2. \tag{16}$$

in the ultra-relativistic limit $\gamma_0 \gg 1$.

3.2.2 Evolution of the relaxation zone

Even though electrons are treated as a collisionless fluid, the presence of a positively charged ion sheet is sufficient

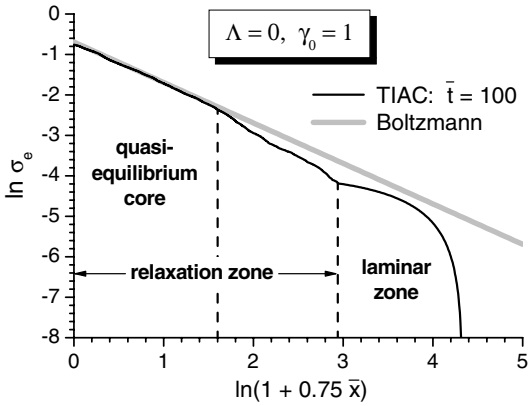

Fig. 4. Spatial profile of the electron column density $\sigma_e(\bar{t},\bar{x})$ as calculated numerically with the TIAC code in the non-relativistic limit for $\bar{t}=100$. The equilibrium profile (20), obtained by using the Boltzmann relation, is shown as a thick grey straight line.

for the electron subsystem to develop a stochastical behavior. Once the electron trajectories in the central region begin to intersect in the process of oscillations across the ion layer (see Fig. 2), their further motion becomes increasingly stochastic. As a result, an isothermal quasi-equilibrium core gradually develops inside the relaxation zone, where the electron density obeys the Boltzmann relation $n_e(x) \propto \exp(e\phi/T)$; here $\phi(x)$ is the equilibrium electrostatic potential, and T is the temperature of the quasi-equilibrium core. This qualitative picture is fully confirmed by the results of direct simulations with the TIAC code presented in Figure 4.

Having adopted the Boltzmann relation, one easily solves the Poisson equation and obtains

$$\bar{\phi}(\bar{x}) = -2\bar{T}\,\ln\left(1+\frac{|\bar{x}|}{4\bar{T}}\right), \tag{17}$$

where $\bar{\phi}$ and $\bar{T}$ are, respectively, the potential in units $m_e v_0^2\gamma_0/e$ and the temperature in units $m_e v_0^2\gamma_0$. The temperature $\bar{T}$ is found from the energy integral (6), which in our case transforms to a transcendental equation

$$2\bar{T}\beta_0^2 + \frac{K_0\left(1/\beta_0\Pi_0\bar{T}\right)}{\gamma_0\,K_1\left(1/\beta_0\Pi_0\bar{T}\right)} = 1; \tag{18}$$

here $K_0(z)$ and $K_1(z)$ are the modified Bessel functions. The limiting values of $\bar{T}$ are

$$\bar{T} = \begin{cases} \dfrac{1}{3}, & \Pi_0 \ll 1, \\ \dfrac{1}{2}, & \Pi_0 \gg 1. \end{cases} \tag{19}$$

Figure 4 compares the equilibrium electron column density [as defined by equation (8)]

$$\sigma_{e,eq}(\bar{x})|_{\bar{x}>0} = \frac{1}{2}\left(1+\frac{\bar{x}}{4\bar{T}}\right)^{-1}, \tag{20}$$

calculated from equation (17), with that obtained from the TIAC numerical simulations in the non-relativistic limit for $\bar{t}=100$. One clearly distinguishes a quasi-equilibrium core of the relaxation zone, which is adequately described by the Boltzmann relation. Departures from the equilibrium are significant in the outer part of the relaxation zone and, of course, in the laminar zone.

To assess practical applicability of our results obtained below for ion acceleration, one needs to know how the boundary $x_r(t)$ between the relaxation and the laminar zones evolves in time. We analyze this evolution by combining an analytical estimate in the limit of $t\to\infty$ with the TIAC simulations for times $\bar{t}\lesssim 100$.

Since randomization of the electron motion in the relaxation zone leads to establishment of the Maxwell-Boltzmann distribution, we can invoke the following argument to evaluate the width $\bar{x}_r$ of this zone at times $\bar{t}\gg 1$: by a time $\bar{t}$ the relaxation zone spreads to a distance $\bar{x}_r$ such that $\bar{t}=N_r\,\bar{t}_{eq}(\bar{x}_r)$, where N_r is a numerical factor of the order unity, and $\bar{t}_{eq}(\bar{x}_r)$ is the travel time between $\bar{x}=0$ and $\bar{x}=\bar{x}_r$ in the equilibrium potential (17) of an electron whose kinetic energy vanishes at $\bar{x}=\bar{x}_r$. In a sense, $t_{eq}(x_r)$ is a timescale on which the information about maxwellization of the velocity distribution up to a certain limiting value v_r is transferred from $x=0$ to the corresponding limiting distance x_r in the infinite potential well (17). This argument sounds perfectly reasonable for the quasi-equilibrium core, and may be surmised to apply to the entire relaxation zone as well.

The time $\bar{t}_{eq}(\bar{x}_r)$ is given by an integral

$$\bar{t}_{eq}(\bar{x}_r) = \int_0^{\bar{x}_r} \frac{d\bar{x}}{\bar{v}_e(\bar{x})}, \tag{21}$$

where the velocity $\bar{v}_e(\bar{x})$ is found from the energy integral

$$\gamma_e(\bar{x}) - 1 = 2\beta_0\Pi_0\bar{T}\,\ln\frac{4\bar{T}+\bar{x}_r}{4\bar{T}+\bar{x}} \tag{22}$$

for an electron moving in the static potential (17). After some algebra we obtain

$$\bar{t}_{eq}(\bar{x}_r) = \frac{4\bar{T}+\bar{x}_r}{\sqrt{\gamma_0\bar{T}}} \int_0^{\sqrt{\ln(1+\bar{x}_r/4\bar{T})}} \frac{1+2\beta_0\Pi_0\bar{T}z^2}{\sqrt{1+\beta_0\Pi_0\bar{T}z^2}}\,e^{-z^2}\,dz. \tag{23}$$

In the asymptotic limit of $\bar{x}_r\gg 1$ equation (23) yields $\bar{t}_{eq}(\bar{x}_r)=\alpha_{eq}\bar{x}_r$, where the numerical coefficient α_{eq} is a weak function of Π_0: $\alpha_{eq}=\sqrt{3\pi}/2$ for $\Pi_0\ll 1$, and $\alpha_{eq}=1$ for $\Pi_0\gg 1$. This leads us to a conclusion that asymptotically the ratio $\bar{x}_r(\bar{t})/\bar{t}$ should approach a certain constant value α_r (or oscillate in a narrow range around this value), which is fully confirmed by the TIAC simulations for times $\bar{t}\le 100$.

Figure 5 shows the temporal dependence of the upper and lower boundaries of the relaxation zone in terms of a hyperbolic variable $\chi_r=\chi_r(\bar{t})$ introduced via a relationship

$$\tanh\chi_r = \frac{x_r(t)}{ct} = \beta_0\frac{\bar{x}_r(\bar{t})}{\bar{t}}. \tag{24}$$

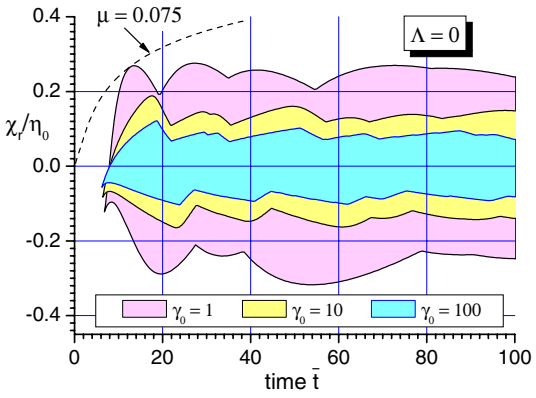

Fig. 5. (Color online) Evolution of the relaxation zone (shaded areas) for $\Lambda = 0$ and three different values of γ_0 in terms of the hyperbolic variable χ_r [see Eq. (24)] normalized to $\eta_0 = \operatorname{arccosh}\gamma_0$ as calculated numerically with the TIAC code. The upper and the lower branches of the $\chi_r(\bar{t})$ curves correspond, respectively, to the boundaries in the upper ($x > 0$) and lower ($x < 0$) half-spaces. Dashed curve is the trajectory of a test ion with $\mu = 0.075$ that barely touches the relaxation zone for $\gamma_0 = 1$.

The fraction of the electron cloud occupied by the upper laminar zone is given by $1 - \chi_r/\eta_0$ [in the ultra-relativistic case the separation along the hyperbolic variable $\chi = \operatorname{arctanh}(x/ct)$ is physically more representative than the separation along x], where $\eta_0 = \operatorname{arccosh}\gamma_0 = \operatorname{arcsinh}\Pi_0$. If $\chi_r(\bar{t})$ should reach the value η_0, it would mean that the relaxation zone has reached the electron front $\bar{x} = \bar{t}$ and the laminar zone has vanished. One clearly sees that typically the electron cloud is not dominated by the relaxation zone, whose fraction asymptotically approaches some constant value, and which has a tendency to shrink with the increasing γ_0. For $\gamma_0 = 1$ this fraction is $\alpha_r = 0.25 \pm 0.02$. Therefore, it can be expected that there exists a sizable window in the parameter space where the test ion acceleration takes place either entirely or predominantly in the laminar zone.

3.3 Solution for $\Lambda > 0$

For a finite-thickness foil it is convenient to introduce a different pair of time and length units,

$$[t] = \Lambda t_\Sigma = \omega_0^{-1}\gamma_0^{1/2}, \quad [x] = \Lambda l_\Sigma = v_0\omega_0^{-1}\gamma_0^{1/2}, \qquad (25)$$

where the time unit $[t]$ is the inverse of the relativistic plasma frequency $\omega_0\gamma_0^{-1/2}$. In these units the frequency and the amplitude of the electron oscillations inside the foil are of the order unity for any value of $\gamma_0 > 1$. Below, the quantities measured in units (25) are marked with a tilde. Note that in these units the dimensionless thickness of the foil is $\tilde{l}_0 \equiv \Lambda$.

3.3.1 Electron trajectories

For subsequent analysis of the test ion motion we need the electron trajectories in the upper half-space $x > 0$. However, because for $\Lambda > 0$ each such trajectory $\tilde{x}_e(\tilde{t}, \tilde{l})$ starts inside the foil at $-\Lambda \le \tilde{x} \le 0$, we should solve equations (5) in this region as well, with the initial conditions $\tilde{x}_e(0, \tilde{l}) = -\tilde{l}$, $\Pi_e(0, \tilde{l}) = \Pi_0$. The required relativistic solution in the laminar zone at $-\Lambda \le \tilde{x}_e \le 0$ has the form

$$\tilde{x}_e(\tilde{t}, \tilde{l}, \beta_0) = -\tilde{l} + h(\tilde{t}, \beta_0), \qquad (26)$$

where $h(\tilde{t}, \beta_0)$ is a periodic function of time $\tilde{t}$; for the first quarter-period it is implicitly given by the quadrature

$$\tilde{t} = \int_0^h \frac{1 - \frac{1}{2}\beta_0^2\zeta^2}{\sqrt{1 - \zeta^2 + \frac{1}{4}\beta_0^2\zeta^4}}\, d\zeta. \qquad (27)$$

This quadrature is in fact a solution for a relativistic particle moving in a quadratic oscillator potential, for which one has the following energy integral

$$\sqrt{1 + \Pi_e^2} + \frac{1}{2}\beta_0\Pi_0\, h^2 = \gamma_0. \qquad (28)$$

From equation (28) one readily establishes that the full amplitude (in units of $v_0\omega_0^{-1}\gamma_0^{1/2}$) of electron oscillations inside the foil is $2h_0$, where

$$h_0 = \left(\frac{2\gamma_0}{\gamma_0 + 1}\right)^{1/2}. \qquad (29)$$

In the non-relativistic limit, obtained by putting $\beta_0 = 0$ in equation (27), we have $h(\tilde{t}) = \sin\tilde{t}$ and $h_0 = 1$.

Now, the trajectory of an electron $\tilde{l}$ in the laminar zone at $x > 0$, which matches the solution (26), (27) at the foil surface $\tilde{x}_e = 0$ at a time $\tilde{t} = \tilde{t}_{e1}$, can be written as

$$\tilde{x}_e(\tilde{t}, \tilde{l}, \beta_0) = \frac{R}{P + \sqrt{P^2 - \beta_0^2\tilde{l}\,R}}, \qquad (30)$$

$$\Pi_e(\tilde{t}, \tilde{l}, \beta_0) = \Pi_0\left[Q - \tilde{l}\,(\tilde{t} - \tilde{t}_{e1})\right], \qquad (31)$$

$$P = P(\tilde{l}, \beta_0) = 1 - \frac{1}{2}\,\beta_0^2\,\tilde{l}^2, \qquad (32)$$

$$Q = Q(\tilde{l}, \beta_0) = \sqrt{1 - \tilde{l}^2 + \frac{1}{4}\,\beta_0^2\,\tilde{l}^4}, \qquad (33)$$

$$R = R(\tilde{t}, \tilde{l}, \beta_0) = (\tilde{t} - \tilde{t}_{e1})\left[2Q - \tilde{l}\,(\tilde{t} - \tilde{t}_{e1})\right], \qquad (34)$$

$$\tilde{t}_{e1} = \tilde{t}_{e1}(\tilde{l}, \beta_0) = \int_0^{\tilde{l}} \frac{1 - \frac{1}{2}\beta_0^2\zeta^2}{\sqrt{1 - \zeta^2 + \frac{1}{4}\beta_0^2\zeta^4}}\, d\zeta; \qquad (35)$$

here the values of $\tilde{l}$ are confined to the interval $0 \le \tilde{l} \le \min\{\Lambda, h_0\}$. The non-relativistic limit of this solution is easily recovered by putting $\beta_0 = 0$. To obtain the electric field in the laminar zone

$$E(\tilde{t}, \tilde{x}) = 4\pi e n_0 v_0 \omega_0^{-1}\gamma_0^{1/2}\, \tilde{l}(\tilde{t}, \tilde{x}), \qquad (36)$$

we need the function $\tilde{l}(\tilde{t}, \tilde{x}, \beta_0)$, which is the inverse of $\tilde{x}_e(\tilde{t}, \tilde{l}, \beta_0)$ with respect to $\tilde{l}$. When calculating the results

discussed in Section 4.2, such inversion of equations (30)–(35) was performed numerically.

Since the values of $\tilde{l}$ lie within the interval $0 \le \tilde{l} \le \Lambda$, a vacuum gap is formed between the ejected electrons and the ion layer in the case of $\Lambda < h_0$ for a limited time after the rear electron edge $\tilde{l} = \Lambda$ reaches the foil surface at $x = 0$ — similar to the case of $\Lambda = 0$ (see Fig. 2) where such a gap exists at $0 < \bar{t} < 2$. Throughout the gap, the electric field E is constant and $\tilde{l} = \Lambda$. To avoid unnecessary technical complications, we exclude the interval $0 < \Lambda < h_0$ from our consideration, i.e. we perform all the calculations either for the limiting case of $\Lambda = 0$, or for $\Lambda > h_0$ when no gap appears between the ejected electrons and the foil ions. The reward is that we get rid of the dependence on Λ in the electric field (36), i.e. $\tilde{l}(\tilde{t}, \tilde{x}, \beta_0)$ becomes a smooth function of $\tilde{t}$ and $\tilde{x}$ (at $\tilde{t} \ge 0$ and $0 \le \tilde{x} \le \tilde{t}$) which does not depend on Λ. In particular, we arrive at an important conclusion that the behavior of the electron trajectories (hence, the distribution of any other physical quantity) in the laminar zone of the electron cloud at $\tilde{x} > 0$ does not depend on Λ for $\Lambda > h_0$.

3.3.2 Evolution of the relaxation zone

The general arguments of Section 3.2.2 on the evolution of the relaxation zone at $\Lambda = 0$ remain valid for $\Lambda > 0$ as well. In particular, these arguments lead us to the following estimate for the relative width of the relaxation zone

$$\left| \frac{\chi_r(t)}{\eta_0} \right| \le \alpha_{\chi r} < \infty, \tag{37}$$

where $\chi_r(t)$ is defined in equation (24), and $\alpha_{\chi r}$ does not depend on time t but is a function of Λ and γ_0. Unfortunately, we have no rigorous proof that one can introduce an upper bound (37) that is valid at all times $t < \infty$. We have only been able to verify it numerically with the TIAC code within a limited range of $\Lambda \lesssim 20$, $\tilde{t} \lesssim 100$. As an example, Figure 6 shows the evolution of the relaxation zone for $\Lambda = 10$ and $\gamma_0 = 1$, 10, and 100.

The TIAC simulations clearly indicate that the relative width of the relaxation zone $\alpha_{\chi r}$ increases with the increasing Λ, and decreases with the increasing γ_0. In particular, in the non-relativistic limit of $\gamma_0 \to 1$ we have $\alpha_{\chi r} > 1$ for $\Lambda > 5.45$, i.e. for $\Lambda > 5.45$ the laminar zone completely vanishes after some time (see Fig. 6). However, it reappears already at moderately relativistic electron energies $\gamma_0 \gtrsim 4$, and becomes quite broad at $\gamma_0 > 10$–100, when we have $\alpha_{\chi r} \lesssim 0.2$–$0.3$. The latter implies that the laminar-zone regime of test ion acceleration should be particularly relevant to highly relativistic electron clouds with $\gamma_0 \gtrsim 100$.

In the previous subsection it was established that the electron trajectories in the laminar zone do not depend on Λ for $\Lambda > h_0$. This, however, does not mean that the same should apply to the boundary between the relaxation and the laminar zones because this boundary is determined by electrons traversing the relaxation zone. Nevertheless,

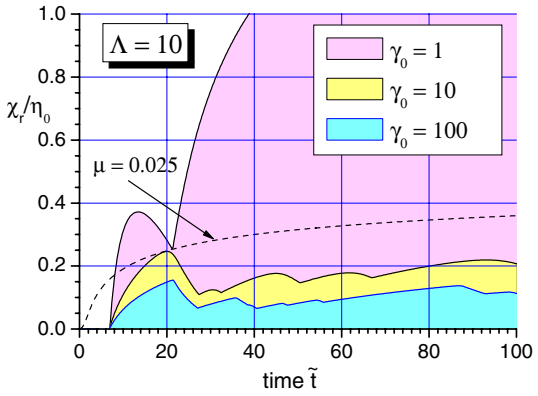

Fig. 6. (Color online) Same as Figure 5 but for an upper half-space $x > 0$ above a foil of finite thickness $\Lambda = 10$. Dashed curve is the trajectory of a test ion with $\mu = 0.025$ that barely touches the relaxation zone for $\gamma_0 = 10$.

one might expect that the curve $\chi_r(\tilde{t})$ should approach some limiting form for a fixed γ_0 and $\Lambda \to \infty$: such a limit would correspond to the case where the bulk plasma ions occupy the entire half-space $x < 0$. However, the existence of such limit for all $t < \infty$ is far from obvious. Numerical simulations show that only the initial portion of the $\chi_r(\tilde{t})$ curve somewhat beyond its first local maximum at $\tilde{t} \simeq 15$–20 (see Figs. 5 and 6) becomes independent of Λ for $\Lambda \gtrsim 2.5$.

4 Motion of test ions

Acceleration of a positive test ion with a charge $+eZ_p$ and a mass m_p (in conventional units) is described by the equations of motion

$$\frac{1}{c}\frac{dx_p}{dt} = \frac{\Pi_p}{\sqrt{1+\Pi_p^2}} \equiv \beta_p, \tag{38a}$$

$$\frac{d\Pi_p}{dt} = +\frac{eZ_p}{m_p c}\, E(t, x_p), \tag{38b}$$

where $x_p(t)$ is the position of the ion, and $\Pi_p(t) = \beta_p\gamma_p = \beta_p(1-\beta_p^2)^{-1/2}$ is its momentum in units of $m_p c$. As a rule, we assume that the test ion starts at $t = t_{p0} = 0$ with the initial values $x_p(t_{p0}) = \Pi_p(t_{p0}) = 0$. Then, because the electric field $E(t, x)$ is non-negative for all $x \ge 0$, we are guaranteed that $x_p(t) > 0$ for all $t > 0$. Equations (38) bring in a dimensionless parameter $\mu = m_e Z_p/m_p$, which contains all the required information about the test ion.

4.1 Solution for $\Lambda = 0$

Here, as in Section 3.2, we use the units (11) and mark thus normalized quantities with a bar. The accelerating electric field $E(\bar{t}, \bar{x})$ in the laminar zone is given by equation (14).

4.1.1 Vacuum phase

When $\Lambda = 0$, a test ion begins its motion by traversing a vacuum gap, where it is accelerated by a constant field $E = 4\pi e\Sigma$ until its trajectory

$$\bar{x}_{p,vac}(\bar{t}) = \frac{1}{\mu\beta_0\Pi_0}\left(\sqrt{1+\mu^2\Pi_0^2\bar{t}^2}-1\right) \tag{39}$$

crosses the rear edge [$\xi = 1$ in Eq. (12b)] of the electron cloud at

$$\bar{t} = \bar{t}_{p1} = \frac{2(1+\mu\gamma_0)}{1+2\mu\gamma_0+\mu^2}, \quad \bar{x} = \bar{x}_{p1} = \bar{x}_{p,vac}(\bar{t}_{p1}) \tag{40}$$

with a momentum $\Pi_{p1} = \mu\Pi_0\bar{t}_{p1}$. The latter values should be used as the initial conditions for further acceleration inside the electron cloud.

4.1.2 Non-relativistic solution

In the non-relativistic limit a general analytical solution is easily found to equations (38). The type of this solution depends on whether the roots λ and $1-\lambda$ of the characteristic equation

$$\lambda^2 - \lambda + 2\mu = 0 \tag{41}$$

are real or complex. In this way a critical value $\mu_* = 1/8$ of the parameter μ is established, which separates the two solution types. For $\mu > 1/8$, when λ is complex, a test ion always catches up with the electron front $\bar{x} = \bar{t}$ and acquires the final velocity $v_{p\infty}$ in excess of the initial electron velocity v_0.

In the physically more interesting case of $\mu < 1/8$ (a sufficiently heavy test ion) the sought for solution of equations (38) is given by

$$\bar{x}_p(\bar{t}) = \bar{t} - C_1\bar{t}^{1-\lambda} + C_2\bar{t}^{\lambda}, \tag{42}$$

where

$$\lambda = \frac{1}{2}\left(1-\sqrt{1-8\mu}\right) \tag{43}$$

is the smaller of the two real roots of equation (41), and the integration constants

$$C_1 = \frac{2^{\lambda}(1-\lambda-\mu)}{(1-2\lambda)(1+\mu)^{1+\lambda}}, \quad C_2 = \frac{2^{1-\lambda}(\lambda-\mu)}{(1-2\lambda)(1+\mu)^{2-\lambda}} \tag{44}$$

are calculated by using the initial conditions (40) with $\gamma_0 = 1$; equation (42) applies at $\bar{t} \geq \bar{t}_{p1} = 2/(1+\mu)$.

Solution (42) reveals the following general features of ion acceleration in the laminar zone. The distance $\bar{t}-\bar{x}_p(\bar{t})$ between the electron front and the accelerated ion increases monotonically with time, i.e. a test ion with $\mu < 1/8$ lags further and further behind the electron front as $t \to \infty$. At the same time, the ion velocity $v_p(t) = dx_p/dt$ monotonically grows in time, and in the formal limit of $t \to \infty$ it asymptotically approaches the initial electron velocity v_0 — as it has been established earlier in reference [20]. The latter, however, occurs on an extremely long timescale $\bar{t}_{ac} \simeq \exp\left(\mu^{-1}/2\right)$, which is beyond any realistic value for protons and other ions with $\mu \leq 1/1836$. From practical point of view, an intermediate asymptotics

$$v_p(t) \approx 2\mu v_0 \ln\left(\frac{2\pi e^2\Sigma}{m_e v_0}\, t\right), \tag{45}$$

inferred from equations (42)–(44) for $\mu \ll 1$ and $1 \ll \bar{t} \ll \exp\left(\mu^{-1}/2\right)$, might be of interest — if not the presence of the relaxation zone. The fact is that solution (42) applies only for ions with $0.0745 \leq \mu < 0.125$ because, as one finds from the TIAC simulations (see Fig. 5), the ion trajectories for $\Lambda = 0$ and $\mu < 0.0745$ penetrate into the relaxation zone. Ions with $\mu \leq 1/1836$ are accelerated deep in the relaxation zone, where the Boltzmann relation leading to the quasi-static potential (17) should be a good approximation; one readily verifies that the potential (17) accelerates ions to much higher (by roughly a factor μ^{-1}) energies than those obtained from equation (45). From this we conclude that the acceleration in the near-front laminar zone of a non-relativistic electron sheath is never important for protons and heavier ions. In Section 4.2 we demonstrate that this conclusion, proved here for $\Lambda = 0$, extends to $\Lambda > h_0$ as well.

4.1.3 Relativistic solution

Analysis of ion motion in the general relativistic case is significantly simplified after we make a transformation from the dynamic variables x_p and Π_p to hyperbolic variables χ and η defined by means of the relationships

$$\tanh\chi = \frac{x_p}{ct} = \beta_0\frac{\bar{x}_p}{\bar{t}}, \quad \sinh\eta = \Pi_p. \tag{46}$$

Accordingly, the initial electron velocity v_0 is represented by a parameter η_0, where $\Pi_0 = \sinh\eta_0$, $\gamma_0 = \cosh\eta_0$, $\beta_0 = \tanh\eta_0$. In terms of these variables equations (38) with the electric field from equation (14) become

$$\frac{d\chi}{d\zeta} = \frac{\cosh\chi}{\cosh\eta}\sinh(\eta-\chi), \tag{47a}$$

$$\frac{d\eta}{d\zeta} = 2\mu\frac{\cosh\chi}{\cosh\eta}\sinh(\eta_0-\chi), \tag{47b}$$

where $\zeta = \ln\bar{t}$. Equations (47) do not contain the independent variable ζ on their right-hand sides, which means that certain key features of the ion motion can be revealed by inspecting the integral curves of the first-order phase equation

$$\frac{d\eta}{d\chi} = 2\mu\frac{\sinh(\eta_0-\chi)}{\sinh(\eta-\chi)} \tag{48}$$

in the (χ,η) plane. Of principal importance here is the singular point $(\chi,\eta) = (\eta_0,\eta_0)$.

First of all note that physically meaningful in our context are the integral curves of equation (48) that lie in the half-plane $\eta > \chi$: this follows from inequality $x_p(t) < v_p t$

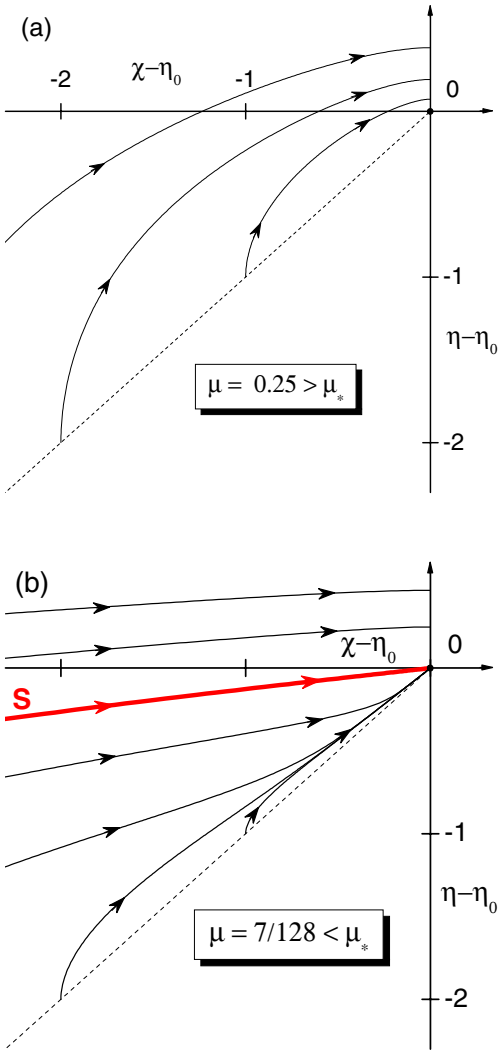

Fig. 7. Phase trajectories for the ion equations of motion in the form (47) in the vicinity of the singular point $(\chi, \eta) = (\eta_0, \eta_0)$ for two values of parameter μ. The singular point is a focus for $\mu > \mu_* = 1/8$ (a), and a node for $\mu < \mu_*$ (b). The separatrix S is a solitary integral curve of equation (48) which enters the node (η_0, η_0) along the direction $\eta - \eta_0 = \lambda(\chi - \eta_0)$, where λ is given by equation (43).

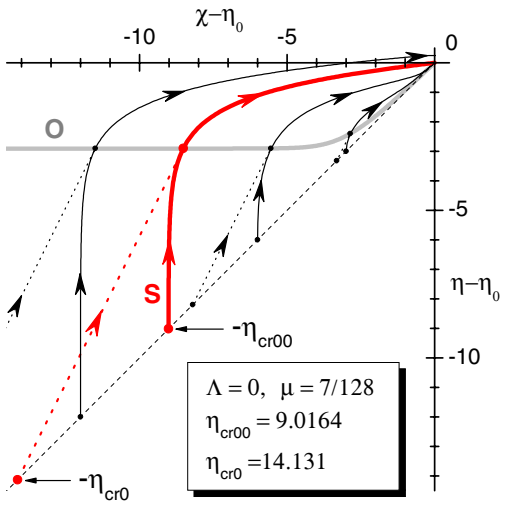

Fig. 8. Global view of the relativistic phase trajectories of a test ion with $\mu = 7/128$. Depending on the ion start delay $\bar{t}_{p0} \geq 0$, the starting point of each trajectory may lie anywhere between its intersection with the grey thick curve O, defined by equations (50), and with the bisector $\eta = \chi$ (dashed line). Straight dotted segments of the phase trajectories correspond to ion acceleration inside the vacuum gap.

valid for any motion with $x_p(0) \geq 0$ and a monotonically increasing velocity $v_p(t)$. The electron front $x = v_0 t$ is represented by the vertical line $\chi = \eta_0$. The ion trajectory can cross the electron front (i.e. the line $\chi = \eta_0$) either in a regular way at $\eta > \eta_0$, or by passing through the singular point (η_0, η_0) along one of the two characteristic directions defined by the characteristic equation (41) (see Fig. 7). A remarkable fact is that the roots of equation (41) do not depend on η_0, i.e. are the same for the relativistic and non-relativistic motions. As a consequence, we obtain a universal critical value $\mu_* = 1/8$ which separates two topologically different patterns of the ion trajectories near the singular point (η_0, η_0).

For light ions with $\mu > 1/8$, when the singular point (η_0, η_0) is a focus (see Fig. 7a), the qualitative picture is the same as in the non-relativistic case: a test ion always reaches the electron front $\chi = \eta_0$ within a finite time interval and crosses it at $\eta > \eta_0$, i.e. with a velocity $v_p = v_{p\infty} > v_0$.

For heavier ions with $\mu < 1/8$ the singular point $(\chi, \eta) = (\eta_0, \eta_0)$ is a node with two entrance directions

$$\eta - \eta_0 = \lambda(\chi - \eta_0), \quad \text{separatrix } S, \tag{49a}$$

$$\eta - \eta_0 = (1 - \lambda)(\chi - \eta_0), \quad \text{general direction}, \tag{49b}$$

where λ is given by equation (43). Note that for $\mu \ll 1$ we have $\lambda \approx 2\mu \ll 1$. The separatrix S divides all the integral curves in the (χ, η) plane into two classes. To the first class belong the curves which lie below the separatrix S in Figures 7b and 8 and enter the singular point along the general direction (49b). From equations (47), (48) and (49b) we infer that $\bar{t} \to \infty$ along such trajectories, as the value of $\eta_0 - \chi$ decreases in proportion to $\bar{t}^{-\lambda}$. In this case, exactly as in the non-relativistic limit, the distance $\bar{t} - \bar{x}_p(\bar{t})$ between the ion and the electron front increases monotonically with time in direct proportion to $\bar{t}^{1-\lambda}$, while the ion momentum $\Pi_p(\bar{t})$ monotonically grows and asymptotically approaches Π_0 on a timescale $\bar{t}_{ac} \simeq \exp\left(\lambda^{-1}\right)$. To the second class belong the trajectories that lie above the separatrix S and cross the electron front $\chi = \eta_0$ at $\eta > \eta_0$. Ions moving along these trajectories catch up with the electron front in a finite time and emerge from the electron cloud with a velocity $v_{p\infty} > v_0$ $(\gamma_{p\infty} > \gamma_0)$.

A qualitative difference between the relativistic and non-relativistic cases arises when one considers the behavior of the separatrix S. In the non-relativistic limit the latter is a straight line given by equation (49a). One can prove that all physically interesting ion trajectories that start at any time $t_{p0} \geq 0$ from $x_p = 0$ with the zero initial

velocity $v_p = 0$ always lie below S, i.e. belong to the first class described in the previous paragraph. The relativistic separatrix, in contrast, bends down and crosses the line $\eta = \chi$ at a certain value $\eta - \eta_0 = \chi - \eta_0 = -\eta_{cr00}$ (see Fig. 8), where $\eta_{cr00} = \eta_{cr00}(\mu)$ is a function of μ. As a consequence, for a given μ and $\eta_0 > \eta_{cr00}(\mu)$ the phase trajectory of a test ion may pass above the separatrix and fall into the second class. In such a case a test ion overtakes the electron front within a finite time interval. To reach more definite conclusions, we have to take a closer look at the initial conditions.

If a test ion begins to move simultaneously with electrons at $t = t_{p0} = 0$, the initial part of its trajectory lies in vacuum and is represented by a segment of a straight line $\eta = \eta_{vac}(\chi) = 2\chi$ [as it follows from Eqs. (39) and (46)] with $0 \le \chi \le \chi_{p1} = \eta_{p1}/2$; in Figure 8 these segments are shown as dotted straight intervals. Then, the initial conditions for the phase equation (48) are given by the values

$$\chi = \chi_{p1} = \frac{1}{2}\eta_{p1}, \tag{50a}$$

$$\eta = \eta_{p1} = \operatorname{arcsinh}\left[\frac{2\mu \sinh\eta_0\ (1+\mu\cosh\eta_0)}{1+2\mu\cosh\eta_0+\mu^2}\right], \tag{50b}$$

inferred from equations (39), (40) and (46). If we fix μ and treat η_0 as a free parameter, equations (50) define a universal curve O in the $(\chi-\eta_0, \eta-\eta_0)$ plane (see Fig. 8) — the locus of the initial points for the integral curves of equation (48). The value of parameter η_0 along the curve O at its intersection with the separatrix S defines the primary critical value $\eta_{cr0} = \eta_{cr0}(\mu)$ for this parameter. Its meaning is as follows: for any $\eta_0 > \eta_{cr0}(\mu)$ a test ion with the charge-over-mass ratio μ finally catches up with the electron front and overtakes it.

The fact that the vacuum segments of the phase trajectories in Figure 8 rise less steeply than the initial portions of the relativistic integral curves of equation (48) suggests that a delayed (at $t_{p0} > 0$) start of a test ion may result in its more efficient acceleration. Such a delayed start may occur when a test positive particle is created on the spot some time after the laser pulse. If we consider a delayed start at $\bar{t}_{p0} \ge 2$, when the vacuum gap is already closed (the opposite extreme to the previously considered case of simultaneous start at $t_{p0} = 0$), the locus of the initial points $(\chi, \eta) = (0, 0)$ for the integral curves of equation (48) in the $(\chi-\eta_0, \eta-\eta_0)$ plane will be the bisector line $\eta - \eta_0 = \chi - \eta_0$. Hence, the intersection of the separatrix S with this bisector defines the secondary critical value $\eta_{cr00} = \eta_{cr00}(\mu) < \eta_{cr0}(\mu)$ of parameter η_0 (see Fig. 8), which has the following meaning: for any $\eta_0 < \eta_{cr00}(\mu)$ a test ion with the charge-over-mass ratio μ always stays behind the electron front for all possible starting times $t_{p0} \ge 0$. In the intermediate case of $\eta_{cr00} < \eta_0 < \eta_{cr0}$ a test ion can either overtake the electron front or stay behind it, depending on the start delay $0 < \bar{t}_{p0} < 2$. A selection of $\eta_{cr0}(\mu)$ and $\eta_{cr00}(\mu)$ values calculated by solving equation (48) numerically is given in Table 1.

Table 1. Critical parameters $\eta_{cr0}(\mu)$, $\eta_{cr00}(\mu)$, and $\eta_{cr\Lambda}(\mu)$ as calculated for a selection of μ values by numerically integrating the ion equations of motion (47).

$1/\mu$	η_{cr0}	η_{cr00}	$\eta_{cr\Lambda}$
10	5.94216	4.51193	5.35497
20	15.7848	9.88926	15.0917
100	94.3602	49.9827	93.6670
200	193.685	99.9916	192.990
1000	992.089	499.998	991.395
2000	1991.40	999.999	1990.71

4.1.4 The ultra-relativistic limit

In the physically important limit of $\mu \ll 1$ the functions $\eta_{cr0}(\mu)$ and $\eta_{cr00}(\mu)$ can be calculated analytically by using the ultra-relativistic ($\mu\Pi_0 \gg 1$) expansion of equations (50) for the curve O in Figure 8,

$$\eta - \eta_0 = \ln\mu, \tag{51}$$

and the integral

$$\exp(\eta - \eta_0) - 2\mu(\chi - \eta_0) = C \tag{52}$$

of equation (48) in the limit of $\eta_0 - \chi \gg 1$, $\eta - \chi \gg 1$, when the right-hand side of equation (48) can be approximated as $2\mu\exp(\eta_0 - \eta)$. Having set the integration constant $C = 1$, we obtain the equation of the separatrix S in the $(\chi - \eta_0, \eta - \eta_0)$ plane. Note that, although derived in the limit of $\eta_0 - \chi \gg 1$, this equation has a correct limiting behavior at $\chi \to \eta_0$ as well. After we calculate the intersection points of the separatrix S with the curve O [as given by Eq. (51)] and with the bisector $\chi = \eta$, we find

$$\eta_{cr0} = \ln\mu + \frac{1}{\mu} - 1, \quad \gamma_{cr0} = \frac{1}{2}\mu\exp\left(\frac{1}{\mu} - 1\right), \tag{53}$$

$$\eta_{cr00} = \frac{1}{2\mu}, \qquad \gamma_{cr00} = \frac{1}{2}\exp\left(\frac{1}{2\mu}\right). \tag{54}$$

The corresponding critical values $\gamma_{cr0}(\mu)$ and $\gamma_{cr00}(\mu)$ of parameter γ_0 are obtained by applying the ultra-relativistic formula $\gamma = \cosh\eta \approx (1/2)\exp\eta$. Comparison with the numerical results from Table 1 shows that for $\mu^{-1} > 20$ the asymptotic formulae (53), (54) for η_{cr0} and η_{cr00} are accurate to within 1.4%.

Making use of the integral (52) with the value of $C = \exp(\eta_\infty - \eta_0) > 1$, we calculate the limiting value $\gamma_{p\infty} = (1/2)\exp\eta_\infty$ of the ion gamma-factor in the case when the ion overtakes the electron front,

$$\gamma_{p\infty} = \begin{cases} \mu\gamma_0\left(1 + \ln\dfrac{2\gamma_0}{\mu}\right), \ \bar{t}_{p0} = 0 \text{ and } \gamma_0 > \gamma_{cr0}(\mu), \\ 2\mu\gamma_0\ln(2\gamma_0), \qquad \bar{t}_{p0} \ge 2 \text{ and } \gamma_0 > \gamma_{cr00}(\mu). \end{cases} \tag{55}$$

This our result for $\gamma_{p\infty}$ differs significantly from the value $\gamma_{p\infty} = 2\gamma_0^2$ calculated earlier in equation (35) of reference [20], which we believe to be erroneous. It should be noted, however, that equation (55) can hardly be of any

practical interest for protons and heavier ions because for $\mu \le 1/1836$ the corresponding values of $\gamma_{cr0} \ge 2.3 \times 10^{793}$ and $\gamma_{cr00} \ge 2.4 \times 10^{398}$ are way too large to be ever encountered in nature.

4.1.5 Intermediate asymptotics for the ion energy

Having established that within our model test ions of common interest, i.e. those with $\mu \le 1/1836$, always stay behind the electron front, and that their dimensionless momentum $\Pi_p(\bar{t})$ approaches the electron value Π_0 on an unrealistically long timescale $\bar{t}_{ac} \simeq \exp\left(\mu^{-1}/2\right)$, a natural step would be to look for an intermediate asymptotics for $\Pi_p(\bar{t})$, valid at $1 \ll \bar{t} \ll \exp\left(\mu^{-1}/2\right)$, that would be applicable to practical situations.

Once we let $\mu \ll 1$ and assume that $\gamma_0 \ll \gamma_{cr00}(\mu)$, we can integrate equation (47b) in the limit of $\bar{t} \gg 1$ by making an approximation $\eta = \chi$, which is valid to the first order in μ along the direction of general approach (49b) to the singular point $(\chi, \eta) = (\eta_0, \eta_0)$. With the initial condition

$$\eta(\zeta_{p1}) = \eta_{p1}, \quad \sinh\eta_{p1} = \Pi_{p1} = \mu\Pi_0\bar{t}_{p1}, \tag{56}$$

where $\zeta_{p1} = \ln\bar{t}_{p1}$ and $\bar{t}_{p1}$ is given by equation (40), the result of this integration reads

$$\tanh\frac{\eta-\eta_0}{2} = \tanh\frac{\eta_{p1}-\eta_0}{2}\,\exp\left[-2\mu(\zeta-\zeta_{p1})\right]. \tag{57}$$

Performing Taylor expansion of equation (57) with respect to the small parameter $0 < 2\mu(\zeta-\zeta_{p1}) \ll 1$, we derive the following asymptotic expression for the ion momentum $\Pi_p(t)$

$$\frac{\gamma_p+\Pi_p}{\gamma_{p1}+\Pi_{p1}} = 1 + \left(\frac{\gamma_0+\Pi_0}{\gamma_{p1}+\Pi_{p1}} - \frac{\gamma_{p1}+\Pi_{p1}}{\gamma_0+\Pi_0}\right)\mu\ln\frac{t}{t_{p1}}, \tag{58}$$

where $\gamma_p = \left(\Pi_p^2+1\right)^{1/2}$ and $\gamma_{p1} = \left(\Pi_{p1}^2+1\right)^{1/2}$. Note that, once $1 \ll \bar{t} \ll \exp\left(\mu^{-1}/2\right)$, equation (58) applies at any degree of relativism of either electrons or a test ion, i.e. any of the three quantities Π_0, Π_{p1}, and Π_p is allowed to be arbitrarily small or large compared to unity. Comparison with numerical integration of equations (47) shows that for $\mu \le 1/1836$ the error of the formula (58) at $1 \le \ln(t/t_{p1}) \le 50$ is typically about 2–4%, and never exceeds 8%. In both the non-relativistic ($\Pi_0 \ll 1$) and the ultra-relativistic ($\mu\Pi_0 \gg 1$) limits equation (58) reduces to a simple expression

$$\Pi_p \approx \Pi_{p1}\left(1+\ln\frac{t}{t_{p1}}\right). \tag{59}$$

4.2 Solution for $\Lambda > h_0$

For practical applications the case of $\Lambda \gtrsim 1$ is generally more important than the limit $\Lambda = 0$ considered so far. As a typical example, it may be noted that a 1 μm foil of solid gold ionized to $z = 50$ with $\gamma_0 = 100$ corresponds to $\Lambda \approx 10$. Here we prove that practically all the qualitative and many quantitative results obtained for $\Lambda = 0$ extend to the case of $\Lambda > h_0$ as well.

In units (25) the equations of ion motion (38) become

$$\beta_0\frac{d\tilde{x}_p}{d\tilde{t}} = \frac{\Pi_p}{\sqrt{1+\Pi_p^2}}, \tag{60a}$$

$$\frac{d\Pi_p}{d\tilde{t}} = \mu\Pi_0\,\tilde{l}(\tilde{t},\tilde{x}_p,\beta_0). \tag{60b}$$

As discussed in Section 3.3, the function $\tilde{l}(\tilde{t},\tilde{x},\beta_0)$ does not depend on Λ at $\Lambda > h_0$, and is a smooth function of its arguments in the entire region $0 \le \tilde{t} < \infty$, $0 \le \tilde{x} \le \tilde{t}$. When the ion starts at $t_{p0} = 0$, we have the initial conditions $\tilde{x}_p(0) = \Pi_p(0) = 0$, and the leading terms in the expansion of the desired solution to equations (60) near $\tilde{t} = 0$ are given by

$$\tilde{x}_p(\tilde{t}) = \frac{1}{6}\mu\gamma_0\,\tilde{t}^3 + O(\tilde{t}^4), \tag{61a}$$

$$\Pi_p(\tilde{t}) = \frac{1}{2}\mu\Pi_0\,\tilde{t}^2 + O(\tilde{t}^3). \tag{61b}$$

Since neither equations (60) nor the pertinent boundary conditions depend on Λ, we conclude that, when expressed in units (25), all the results on ion acceleration in the laminar zone are independent of Λ for $\Lambda > h_0$.

The next important point is that in the limit of $\tilde{t} \to \infty$ equations (60) become exactly equivalent to the corresponding equations of motion for $\bar{x}_p(\bar{t})$, $\Pi_p(\bar{t})$ in the case of $\Lambda = 0$. To verify this, we note that equations (30)–(35) imply $\tilde{l} \sim 2/\tilde{t} \ll 1$ for $\tilde{t} \gg 1$. Then, by expanding equations (30)–(35) in powers of $\tilde{l}$, we derive an explicit formula

$$\tilde{l}(\tilde{t},\tilde{x},\beta_0) \approx 4(\tilde{t}-\tilde{x})\Big\{\tilde{t}^2 - \beta_0^2\tilde{x}^2 + 2 + \left[(\tilde{t}^2-\beta_0^2\tilde{x}^2-2)^2 + 8(1-\beta_0^2)\tilde{t}\tilde{x}\right]^{1/2}\Big\}^{-1}, \tag{62}$$

which is valid for any $0 < \beta_0 < 1$ in the limit of $\tilde{l} \ll 1$, and which is further simplified to

$$\tilde{l}(\tilde{t},\tilde{x},\beta_0) \approx \frac{2(\tilde{t}-\tilde{x})}{\tilde{t}^2-\beta_0^2\tilde{x}^2} \tag{63}$$

for $\tilde{t} \gg \gamma_0$ and $0 \le \tilde{x} \le \tilde{t}$. Substituting equation (63) into equation (60b), we obtain exactly the same equations of ion motion in terms of $\tilde{x}_p(\tilde{t})$, $\Pi_p(\tilde{t})$ as those in terms of $\bar{x}_p(\bar{t})$, $\Pi_p(\bar{t})$ for $\Lambda = 0$, which are then reduced to the same phase equation (48) with the same topology of integral curves in the vicinity of the singular point $(\chi, \eta) = (\eta_0, \eta_0)$. As a consequence, we arrive at conclusions that are fully analogous to those made for the case of $\Lambda = 0$:

(i) test ions with $\mu > \mu_* = 1/8$ always catch up and overtake the electron front, being finally accelerated to $\Pi_{p\infty} > \Pi_0$;

(ii) for any $\mu < 1/8$ there exists a critical value $\eta_{cr\Lambda}(\mu)$ of parameter η_0 [or, equivalently, a critical value $\gamma_{cr\Lambda}(\mu)$ of parameter γ_0] such that for any $\eta_0 > \eta_{cr\Lambda}(\mu)$ a test ion with the charge-over-mass ratio μ overtakes the electron front and attains $\Pi_{p\infty} > \Pi_0$; for $\eta_0 < \eta_{cr\Lambda}(\mu)$ and no start delay ($t_{p0} = 0$) the ion lags behind the electron front, while its dimensionless momentum $\Pi_p(\tilde{t})$ asymptotically approaches Π_0 on a timescale $\tilde{t}_{ac} \simeq \exp\left(\mu^{-1}/2\right)$.

These conclusions are fully confirmed by numerical integration of equations (60) with $\tilde{l}(\tilde{t}, \tilde{x}, \beta_0)$ calculated from equations (30)–(35).

A remarkable fact is that we have two universal functions, namely, $\eta_{cr0}(\mu)$ for $\Lambda = 0$, and $\eta_{cr\Lambda}(\mu)$ for $\Lambda > h_0$, which cover the entire range of Λ variation. Since at intermediate times $\tilde{t} \simeq 1$ the two cases of $\Lambda = 0$ and $\Lambda > h_0$ are mathematically not equivalent, the functions $\eta_{cr0}(\mu)$ and $\eta_{cr\Lambda}(\mu)$ numerically differ from one another, except for the initial point $\eta_{cr0}(\mu_*) = \eta_{cr\Lambda}(\mu_*) = 0$. This difference, however, is practically not significant, as can be verified by comparing the numerically calculated values of $\eta_{cr0}(\mu)$ and $\eta_{cr\Lambda}(\mu)$ in Table 1. In the limit of $\mu \ll 1$ we derive an asymptotic expression

$$\gamma_{cr\Lambda} = \frac{1}{4}\mu \exp\left(\frac{1}{\mu} - 1\right), \tag{64}$$

which is exactly one half of the corresponding limit (53) for γ_{cr0}. It can be safely conjectured that in the intermediate range $0 < \Lambda < h_0$ the corresponding critical values of γ_0 lie between $\gamma_{cr0}(\mu)$ and $\gamma_{cr\Lambda}(\mu)$. For $\gamma_0 > \gamma_{cr\Lambda}(\mu)$, when a test ion does overtake the electron front, its final energy in the limit of $\mu \ll 1$ is given by

$$\gamma_{p\infty} = \mu\gamma_0\left(1 + \ln\frac{4\gamma_0}{\mu}\right). \tag{65}$$

The approximation (63) yields the same intermediate asymptotics (58) for the ion momentum $\Pi_p(t)$ as in the case of $\Lambda = 0$. The only difference between the two cases is in the initial values t_{p1}, $\Pi_{p1} = \Pi_p(t_{p1})$ to be used in equation (58). Unlike in the $\Lambda = 0$ case, no appropriate analytical solution to equations (60) was found for $\tilde{t} \lesssim 1$ that would yield suitable expressions for $\tilde{t}_{p1}$ and Π_{p1}. It is only in the ultra-relativistic limit $\mu\Pi_0 \gg 1$ that one obtains a simple result $\Pi_{p1} = \mu\Pi_0$, $\tilde{t}_{p1} = (\mu\gamma_0/2)^{1/2}$. In the opposite limit of $\mu\Pi_0 \ll 1$ expansion (61b) suggests that the value $\Pi_p = \mu\Pi_0$ is achieved at $\tilde{t} \simeq 1$. Taking guidance from such considerations, we propose simple approximate expressions

$$\Pi_{p1} = \mu\Pi_0, \quad \tilde{t}_{p1} = \left(2 + \frac{1}{2}\mu\gamma_0\beta_0^2\right)^{1/2}, \tag{66}$$

which, on the one hand, agree with the ultra-relativistic limit and, on the other hand, fit reasonably well the results of numerical integration of equations (60) (see Fig. 9). As a result, equation (58) with Π_{p1} and $\tilde{t}_{p1}$ taken from equation (66) is formally applicable at $\tilde{t}_{p1} \ll \tilde{t} \ll \exp\left(\mu^{-1}/2\right)$.

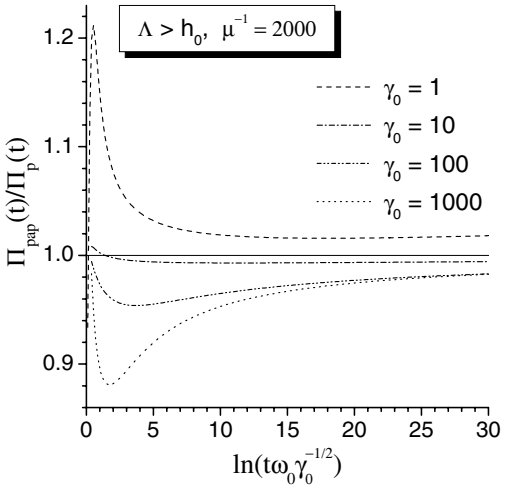

Fig. 9. Comparison of the intermediate asymptotics (58) with the results of numerical integration of the ion equations of motion (60) for $\mu = 1/2000$ and four different values of γ_0: plotted is the ratio of the ion momentum $\Pi_{pap}(t)$, obtained from equations (58) and (66), to the numerically calculated value $\Pi_p(t)$ versus time t in units (25).

A comparison with numerical results in Figure 9 shows that at $\tilde{t} \gtrsim 100$ the intermediate asymptotics (58) has a typical error of a few percent.

If we consider now the case of a delayed ion start at $t = t_{p0} > 0$, we find that for $\tilde{t}_{p0} \gg 1$ we have $\tilde{l} \ll 1$ for all $\tilde{t} \geq \tilde{t}_{p0}$, which again leads us to the approximation (63) and to the phase equation (48) with the initial condition $(\chi, \eta) = (0, 0)$. Hence, for $\tilde{t}_{p0} \gg 1$ the critical value of the η_0 parameter is given by the same function $\eta_{cr00}(\mu)$ as in the $\Lambda = 0$ case. This conclusion is also fully confirmed by numerical integration of equations (60). For $\mu \ll 1$ the dependence of the critical η_0 on the ion start delay $\tilde{t}_{p0}$ is as follows: as $\tilde{t}_{p0}$ increases from $\tilde{t}_{p0} = 0$ to $\tilde{t}_{p0} = \sqrt{2}$, the critical value of η_0 decreases from $\eta_{cr\Lambda}(\mu)$ to $\eta_{cr00}(\mu)$, and for $\tilde{t}_{p0} > \sqrt{2}$ it remains equal to $\eta_{cr00}(\mu)$. In general, when η_0 falls into the range $\eta_{cr00}(\mu) < \eta_0 < \eta_{cr\Lambda}(\mu)$, a test ion can either overtake or stay behind the electron front depending on the value of the start delay t_{p0}.

4.3 Domain of applicability of the laminar-zone solution

The foregoing analysis of ion acceleration was based on the assumption that the ion trajectories lie entirely inside the laminar zone of the electron sheath. As already mentioned in Section 3, this is true only within a certain domain of our three-dimensional parameter space (μ, γ_0, Λ). Because of a weak dependence on Λ, the limits of this domain can be conveniently analyzed in the two-dimensional (μ^{-1}, η_0) plane.

Let $\eta_{lam}(\mu)$ be the threshold value of η_0 at which the trajectory of an ion with a given charge-over-mass ratio μ just touches the outer boundary of the relaxation zone (see Figs. 5 and 6), i.e. for $\eta_0 > \eta_{lam}(\mu)$ the ion trajectory

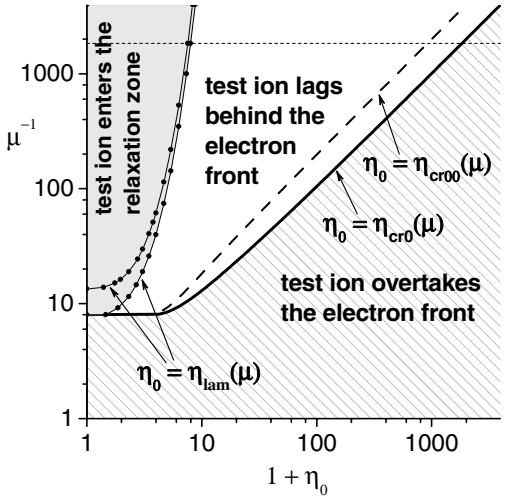

Fig. 10. Characteristic regions in the (η_0, μ^{-1}) parameter plane. Domain of applicability of the laminar-zone solution lies outside the grey shaded area delimited by the two $\eta_{lam}(\mu)$ curves, the inner one calculated for $\Lambda = 0$, and the outer one for $\Lambda = 10$. Hatched region is where test ions overtake the electron front: it is delimited by the $\eta_{cr0}(\mu)$ curve which is practically indistinguishable from $\eta_{cr\Lambda}(\mu)$. Dashed horizontal line corresponds to the proton value $\mu^{-1} = 1836$.

lies entirely in the laminar zone, and for $\eta_0 < \eta_{lam}(\mu)$ it penetrates (at least partially) into the relaxation zone. Typically this touching occurs near the first local maximum of the corresponding $\chi_r(t)$ curve at $\bar{t}, \tilde{t} \simeq 15$–$20$ and lies within the reach of the TIAC code. Because this early part of the boundary between the two zones ceases to depend on Λ for $\Lambda \gtrsim 2.5$, the same applies to the function $\eta_{lam}(\mu)$.

Figure 10 shows two curves $\eta_{lam}(\mu)$, calculated for $\Lambda = 0$ and 10, which actually span the entire dependence of η_{lam} on the Λ parameter. The domain of applicability of the laminar-zone solution lies outside the grey shaded area bounded by the $\eta_{lam}(\mu)$ curves. For protons with $\mu = 1/1836$ it corresponds to $\gamma_0 > 348$ at $\Lambda = 0$, and to $\gamma_0 > 537$ at $\Lambda \gtrsim 2.5$. The fact that the two critical values $\eta_{cr0}(\mu)$ and $\eta_{cr00}(\mu)$ turn out to be deeply inside this domain (at least for $\mu < 0.1$) justifies all the conclusions made in Sections 4.1 and 4.2 about the possibility for a test ion to catch up with the electron front. Note that the two curves $\eta_{cr0}(\mu)$ and $\eta_{cr\Lambda}(\mu)$, which span the dependence of the critical η_0 on the Λ parameter, are virtually indistinguishable in Figure 10.

For protons and heavier ions with $\mu \leq 1/1836$ the following conclusions can be drawn from Figure 10. The position of the $\eta_{lam}(\mu)$ curves indicates that ion acceleration in the non-relativistic case of $\Pi_0 \ll 1$ takes place deeply inside the relaxation zone, where one can expect the usual Boltzmann relation to be a good approximation. The laminar-zone solution is not applicable in such a case. However, it becomes fully applicable when the electrons are boosted to ultra-relativistic energies of $\gamma_0 \gtrsim 300$–500 ($\eta_0 \gtrsim 6$–7).

5 Conclusion

In this paper rigorous results are presented for a particular case of the TNSA mechanism of ion acceleration in a planar electron sheath evolving from an initially mono-energetic cloud of hot electrons. Self-consistent treatment of the collisionless electron dynamics fully captures the effects of departure from the Maxwell-Boltzmann distribution. These effects come to a foreground in the outer laminar zone of the expanding electron cloud, where the ion acceleration can be analyzed by analytical means. In particular, the limiting (in the limit of $t \to \infty$) gamma-factor $\gamma_{p\infty}$ of accelerated test ions can be calculated exactly. Note that the assumption of an isothermal Boltzmann distribution for hot electrons leads to an infinite value of $\gamma_{p\infty}$.

It is shown that the limiting value $\gamma_{p\infty}$ is determined primarily by the values of the two (out of the total three) principal dimensionless parameters of the problem, the ion-electron charge-over-mass ratio $\mu = m_e Z_p / m_p$, and the initial gamma-factor γ_0 of the accelerated electrons. For $\mu > \mu_* = 1/8$ a test positive particle (for example a positron) always overtakes the electron front and reaches $\gamma_{p\infty} > \gamma_0$. In the physically more interesting case of $\mu < \mu_*$ the limiting ion energy depends on whether γ_0 is above or below a certain critical value $\gamma_{cr} = \gamma_{cr}(\mu)$, namely, we have $\gamma_{p\infty} = \gamma_0$ for $\gamma_0 < \gamma_{cr}$, and $\gamma_{p\infty} > \gamma_0$ [as given by Eqs. (55) and (65)] for $\gamma_0 > \gamma_{cr}$. Practically insignificant dependence of γ_{cr} on the dimensionless foil thickness Λ is limited to a variation within a factor 2 and spanned by the functions $\gamma_{cr0}(\mu)$ and $\gamma_{cr\Lambda}(\mu)$ calculated in Table 1 and equations (53) and (64).

In the present model the protons and heavier ions, which have $\mu \leq 1/1836$, can never catch up with the electron front because the corresponding values of $\gamma_{cr} \sim \exp(\mu^{-1})$ are enormous and beyond practical reach. Although formally the ion gamma-factor $\gamma_p(t)$ in this case still tends to γ_0 as $t \to \infty$, this fact is practically irrelevant because $\gamma_p(t)$ approaches γ_0 on an enormous timescale $t_{ac} \simeq t_\Sigma \exp\left(\mu^{-1}/2\right)$ [or $t_{ac} \simeq \omega_0^{-1}\sqrt{\gamma_0}\exp\left(\mu^{-1}/2\right)$ for $\Lambda > 1$] that never occurs in real world. For practical applications one should use the intermediate asymptotic formula (58) derived for dimensionless times $1 \ll \bar{t}, \tilde{t} \ll \exp\left(\mu^{-1}/2\right)$.

The present results for ion motion have been obtained under the condition that the ion trajectory lies entirely in the laminar zone of the electron sheath. Numerical investigation of the laminar zone boundaries reveals that this condition imposes a lower bound $\gamma_0 > \gamma_{lam}(\mu)$ on the initial gamma-factor of hot electrons (see Fig. 10). The latter inequality reflects a more general fact that the role of the non-Boltzmann effects in ion acceleration increases with γ_0, i.e. with the energy of hot electrons. In particular, acceleration of protons by a non-relativistic electron sheath occurs practically entirely in its quasi-Boltzmann core, where the details of the initial electron energy distribution are "forgotten". By contrast, in the ultra-relativistic case of mono-energetic electrons with $\gamma_0 \gtrsim 300$–500, acceleration of protons takes place entirely in the non-Boltzmann laminar zone of the electron sheath, where full memory of the initial electron energy distribution has been preserved.

One more constraint that should not be forgotten is the geometry of the plasma flow. The present treatment has been confined to the purely one-dimensional planar case. In laser-plasma experiments the irradiated area always has some finite transverse dimensions $\simeq d_f$. Clearly, as a test ion travels a distance $x_p \simeq d_f$, the electron sheath can no longer be treated as planar and the effects of flow divergence come into play, which terminate the ion energy growth predicted by the planar solution (as is, for example, illustrated by the self-similar solution in Ref. [13]). Here, however, one can take advantage of the weak (logarithmic) time dependence of the ion energy in the intermediate asymptotics (58): having substituted the value of t by which the ion travels the distance $x_p(t) \simeq d_f$, one can obtain a fairly accurate estimate for the maximum energy of accelerated ions in realistic situations.

The author gratefully acknowledges many stimulating discussions with M. Murakami.

References

1. E.L. Clark et al., Phys. Rev. Lett. **84**, 670 (2000); E.L. Clark et al., Phys. Rev. Lett. **85**, 1654 (2000)
2. A. Maksimchuk et al., Phys. Rev. Lett. **84**, 4108 (2000)
3. R.A. Snavely et al., Phys. Rev. Lett. **85**, 2945 (2000)
4. M. Hegelich et al., Phys. Rev. Lett. **89**, 085002 (2002)
5. T.E. Cowan et al., Phys. Rev. Lett. **92**, 204801 (2004)
6. G.A. Mourou, T. Tajima, S.V. Bulanov, Rev. Mod. Phys. **78**, 309 (2006)
7. S.P. Hatchett et al., Phys. Plasmas **7**, 2076 (2000)
8. S.C. Wilks et al., Phys. Plasmas **8**, 542 (2001)
9. A.V. Gurevich, L.V. Pariiskaya, L.P. Pitaevskii, Zh. Eksp. Teor. Fiz. **49**, 647 (1965) [Sov. Phys. JETP **22**, 449 (1966)]
10. P. Mora, Phys. Rev. Lett. **90**, 185002 (2003)
11. S. Betti, F. Ceccherini, F. Cornolti, F. Pegoraro, Plasma Phys. Control. Fusion **47**, 521 (2005)
12. Yu.V. Medvedev, Plasma Phys. Control. Fusion **47**, 1031 (2005)
13. M. Murakami, M.M. Basko, Phys. Plasmas **13**, 012105 (2006)
14. S. Gitomer et al., Phys. Fluids **29**, 2679 (1986)
15. J.E. Crow, P.L. Auer, J.E. Allen, J. Plasma Phys. **14**, 65 (1975)
16. M. Passoni, V.T. Tikhonchuk, M. Lontano, V.Yu. Bychenkov, Phys. Rev. E **69**, 026411 (2004)
17. J.S. Pearlman, R.L. Morse, Phys. Rev. **40**, 1652 (1978)
18. Y. Kishimoto et al., Phys. Fluids **26**, 2308 (1983)
19. M. Passoni, M. Lontano, Laser Part. Beams **22**, 163 (2004)
20. S.V. Bulanov et al., Plasma Phys. Rep. **30**, 18 (2004)